DOI: 10.1002/cssc.201402055

High-Power Lithium-Ion Capacitor using $LiMnBO_3$-Nanobead Anode and Polyaniline-Nanofiber Cathode with Excellent Cycle Life

Kaliyappan Karthikeyan,*[a, b] Samuthirapandian Amaresh,[a] Sol-Nip Lee,[a] Jae-Yeon An,[a] and Yun-Sung Lee*[a]

$LiMnBO_3$ nanobeads (LMB-NB) with uniform size and distribution were synthesized using a urea-assisted microwave/solvothermal method. The potential application of LMB-NBs as an anode for a lithium-ion hybrid capacitor (Li-AHC) was tested with a polyaniline-nanofiber (PANI-NF) cathode in a nonaqueous $LiPF_6$ (1 M)–ethylene carbonate/dimethyl carbonate electrolyte. Cyclic voltammetry (CV) and charge–discharge (C/DC) studies revealed that the PANI-NF/LMB-NB cell showed an exceptional capacitance behavior between 0–3 V along with a prolonged cycle life. A discharge capacitance of about 125 $F g^{-1}$, and energy and power densities of about 42 $Wh kg^{-1}$ and 1500 $W kg^{-1}$, respectively, could be obtained at a current density of 1 $A g^{-1}$; those Li-AHC values are higher relative to cells containing various lithium intercalation materials in nonaqueous electrolytes. In addition, the PANI-NF/LMB-NB cell also had an outstanding rate performance with a capacitance of 54 $F g^{-1}$ and a power density of 3250 $W kg^{-1}$ at a current density of 2.25 $A g^{-1}$ and maintained 94% of its initial value after 30 000 cycles. This improved capacitive performance with an excellent electrochemical stability could be the result of the morphological features and inherent conductive nature of the electroactive species.

Introduction

Due to the depletion of oil resources and the emergence of hybrid electrical vehicles (HEVs), many efforts are being made to develop new storage devices that are capable of delivering high energy and power densities.[1] Although secondary batteries and electrochemical double-layer capacitors (EDLC) are considered as promising storage devices for such applications, the low power density (PD) of secondary batteries and limited energy density (ED) of EDLCs hinders their application in HEVs. Recently, a new class of supercapacitors called asymmetric hybrid capacitors (AHCs) has been attracting much attention because of their higher ED and PD values relative to EDLCs.[2] These capacitors can be fabricated using different electrode materials with different operating voltages. Moreover, two different storage mechanisms (both supercapacitors and advanced batteries) are involved in AHCs, a fact that also increases the overall cell potential, resulting in higher ED and PD values of a single cell.[3] The construction of AHCs could be performed with various combinations including conductive polymer (CP)/metal oxide (MO),[4] MO/carbon materials,[5] and CP/carbon materials.[6] Among the AHC configurations, MO/carbon-based AHCs were extensively studied.[7] Although RuO_2 is considered as the best electroactive material for fabricating AHCs due to its large pseudocapacitance, energy density, and excellent electrochemical reversibility, its high cost and toxic nature hindered its practical applications.[8] Most recently, many one-dimensional metal oxides (ODMs), such as SnO_2, Fe_2O_3, MnO_2, and TiO_2 among others, have been proposed for pseudocapacitor applications.[7,9–12] Despite showing almost the same pseudocapacitance performance as RuO_2 with less cost and low toxicity, all these ODMs show low conductivity, high metal dissolution during electrochemical cycling, and low redox potential, affecting their high-rate performance, which made ODMs inappropriate for AHC applications. Moreover, the ED of AHCs is directly proportional to cell voltage and capacitance according to Equation (1):

$$E = 1/2\,C\,V^2 \quad (1)$$

where C is capacitance ($F g^{-1}$) and V is cell voltage (V). Because ED can be enhanced by increasing the operating voltage and capacitance of electroactive materials, the low redox potential of ODM also restricted the construction of high-ED AHCs.[13] Hence, further studies have focused on finding novel alternative materials with higher operating voltage values for AHC construction. Recently, the assembly of AHCs with a lithium insertion electrode (battery type) as an energy source and an EDLC component as a power source in either aqueous or non-

[a] Dr. K. Karthikeyan, S. Amaresh, S.-N. Lee, J.-Y. An, Prof. Y.-S. Lee
Faculty of Applied Chemical Engineering
Chonnam National University
Gwang-ju 500-757 (Korea)
Fax: (+82) 62-530-1904
E-mail: leeys@chonnam.ac.kr
kkaliyap@uwo.ca

[b] Dr. K. Karthikeyan
Department of Mechanical and Materials Engineering
The University of Western Ontario
London, Ontario, N6A 5B9 (Canada)

Supporting Information for this article is available on the WWW under http://dx.doi.org/10.1002/cssc.201402055.

aqueous media was achieved.[14] Such lithium-ion AHCs (Li-AHCs) can provide a larger ED than AHCs or EDLCs, and a higher PD than lithium-ion batteries (LIBs), along with stable long-term cycling. Although several lithium intercalation materials have been widely studied for Li-AHCs in aqueous electrolytes, water-splitting of aqueous electrolytes occurred at 1.2 V, confining their ED value. Therefore, the fabrication of Li-AHCs in inorganic electrolytes has been a significant focus.[14] Amatucci et al. first reported a nonaqueous Li-AHC using an activated carbon (AC) positive electrode and a $Li_4Ti_5O_{12}$ negative electrode in a $LiPF_6$–ethylene carbonate (EC)/dimethyl carbonate (DMC) electrolyte.[14,15] Later, numerous lithium-intercalation-based electrodes were studied and reported by several researchers.[16–27] So far, Mn-based lithium intercalating components have been observed as promising energy sources for Li-AHC applications owing to their natural abundance, low environmental impact, and low cost. Unfortunately, Mn-based cathode materials undergo large capacitance fading as a result of active species dissolution either in pristine or doped form and also have low conductivity.[27] Previously, we reported new classes of lithium insertion host materials, such as polyanion framework Li_2MSiO_4 (M = Mn and Fe) and fluoro oxyanion Li_2CoPO_4F as potential energy sources for Li-AHCs along with AC counter electrodes. However, the ED and PD of these materials were still not adequate to power HEVs.[21–23] Therefore, investigations are still going on to develop appropriate high-performance lithium insertion hosts for Li-AHC applications.

Lithium metal borate ($LiMBO_3$, M = Mn or Fe) is proposed as a promising cathode material for LIB applications due to its higher theoretical capacity (< 220 mAh) relative to other electrode materials, such as $LiMO_2$ (M = Co, Ni, Mn, and Fe) and $LiFePO_4$.[28] Likewise, boron is environmentally benign, lightweight, and naturally abundant. Besides, triangular $(BO_3)^{3-}$ polyoxanions have a lighter mass relative to other lithium intercalation materials containing transition-metal polyoxanion compounds with $(XO_m)^{n-}$ groups, such as $(SO_4)^{2-}$, $(VO_4)^{2-}$, $(PO_4)^{2-}$, $(AsO_4)^{2-}$, $(WO_4)^{2-}$, and (SiO_4).[2,29] In addition, $(BO_3)^{3-}$ polyoxanions could deliver high output potentials along with improved structural stability from the inductive effect of the B–O bond. Legagneur et al. first reported the successful utilization of $LiMBO_3$ (M = Mn or Fe) for LIBs with low discharge capacity and poor lithium intercalation/deintercalation reaction kinetics.[29] Although $LiFeBO_3$ (LFB) is safer than $LiMnBO_3$ (LMB), the higher theoretical capacity and higher output potential (~4.6 V) of LMB relative to LFB (~3.2 V) makes LMB more attractive as a candidate for LIBs. Nevertheless, due to the low electrical and ionic conductivity of LMB, several valid attempts are needed to improve electrochemical performance including conductive carbon coating or foreign cation doping, which also results in detrimental side reactions from the addition of nonreactive materials. Various studies on LMB as a cathode material for LIBs indicated the existence of LMB in two phases, either hexagonal (h-LMB) or monoclinic (m-LMB).[28,30] Ma et al. studied the anodic performance of h-LMB between 0 and 3 V, showing a stable cyclic life with a discharge capacity of approximately 354 mAh g^{-1} at a current density of 50 mA g^{-1}.[31] There are still some setbacks, such as low electronic conductivity and low rate performance, which need several valid developments and strategies to improve the electrochemical performance of LMB for next-generation LIBs. Therefore, we now focus on one interesting factor of LMB that shows excellent capacity retention at the lower voltage region of 0–3 V because of its adjustable voltage-platform characteristics.[31] To the best of our knowledge, no other report is available on the utilization of LMB as an electroactive material for Li-AHCs. Thus, herein we present LMB as a high-performance anode material for Li-AHCs.

Generally, carbonaceous materials are the most common electrode materials for Li-AHCs. However, their low capacitance, low bulk density, poor charge-storage capability, and risk of high-surface-area lithium plating at high current densities restrict them in high-energy-density Li-AHC applications.[32] Consequently, ODM and its derivatives were used for such applications, which also underwent active species dissolution and had a low redox potential. Consequently, an alternative counter electrode with a high working voltage and high capacitance was sought.[10,12] Employing CPs as counter electrodes is the best way to increase the capacitive behavior of AHCs.[6,7,12,33] Moreover, polyaniline (PANI) is the most promising electrode material for AHCs, owing to its controllable electrical conductivity in its oxidized/protonated form, its environmental stability, low cost, and easy synthesis.[33] Furthermore, PANI also exhibited higher capacitance and redox potential than AC and several ODMs, improving the overall performance of the Li-AHC system. Although CPs are well-known for their poor electrochemical cyclability, various approaches have been reported for assembling AHCs with CP as an active material and enhanced cycling performance.[6,34,35] In our earlier work, we studied a hybrid composite containing a PANI–lithium intercalating material as a high-performance cathode for Li-AHCs with a high ED value and a long cycling performance.[26] Herein, we present a novel Li-AHC with a LMB anode and a PANI cathode in a $LiPF_6$ (1 M)–EC/DMC electrolyte with an improved rate performance and a long cycle life. This approach will be a promising technique for assembling highly efficient Li-AHCs for HEVs.

Results and Discussion

Figure 1 presents the XRD pattern of LMB nanobeads (LMB-NBs) prepared at 650 °C for 7 h under an Ar atmosphere. LMB-NBs had a monoclinic phase with the *C*2/*c* space group, which is isostructural to $LiCdBO_3$ (according to ICDD card no. 83–2342) and also in good agreement with earlier reports.[28–30] LMB-NBs are mainly constructed from planar BO_3, tetrahedral LiO_4, and MnO_5 square pyramids. Usually, the planar BO_3 group is linked by edge-sharing and Li ions occupy LiO_4 tetrahedral sites in the 3D polyanionic $[MnBO_3]_n^{n-}$ framework.[30] The MnO_5 square pyramid is formed of chains along with the *c* axis by sharing its opposite edges with two adjacent pyramids.[29] In addition, the tetrahedral sites of LiO_4 shared two oxygen and planar BO_3 groups, forming a chain through corner-sharing. Because the Li atom in LMB occupied LiO_4 tetrahedral sites and shared a face with an oxygen atom, the electronic conduction

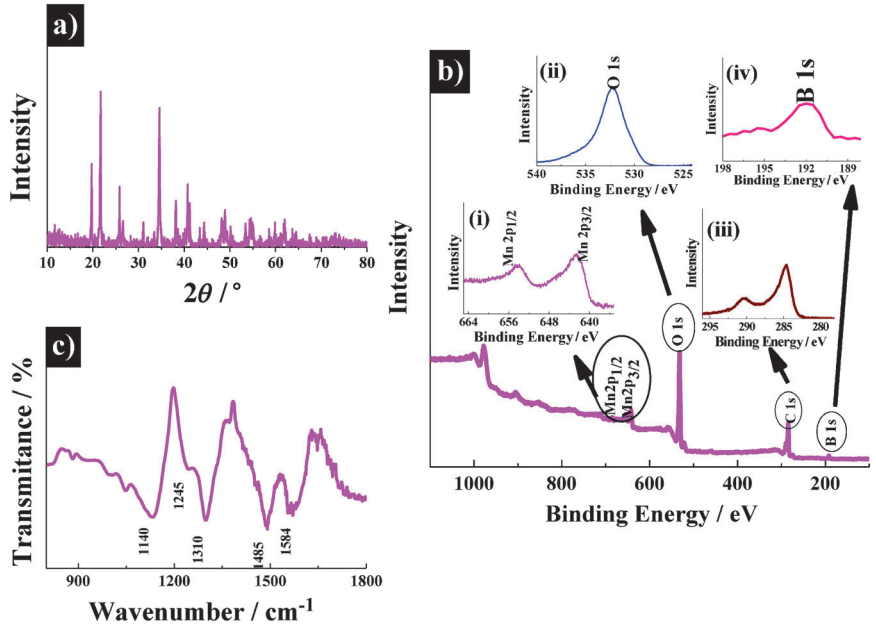

Figure 1. a) XRD pattern and b) XPS spectra of LMB-NBs prepared at 650 °C for 7 h under Ar; inset shows high-resolution XPS spectra of corresponding elements. c) FTIR spectra of PANI-NFs prepared by the chemical polymerization method at room temperature.

of LMB was followed by Mn–O–Mn bonding, resulting in poor electronic conductivity.[29,30] Moreover, the narrow and intense XRD peaks demonstrated the good crystalline nature of LMB-NBs. The lattice parameters calculated from XRD analyses (a = 5.192 Å, b = 8.944 Å, and c = 10.328 Å) were close to the values reported elsewhere.[28,30] X-ray photoelectron spectroscopy (XPS) analysis of LMB-NBs was carried out to obtain information on surface composition. XPS spectra of LMB-NBs (Figure 1 b) show the presence of Mn, C, B, and O elements within the sample. The predominant peaks at 642.5 and 654.1 eV in high-resolution Mn 2p spectra can be attributed to Mn $2p_{1/2}$ and Mn $2p_{3/2}$ core levels, respectively.[36] The high-resolution C 1s XPS spectrum of LMB-NBs showed the C 1s peak of the epoxy group at 286.7 eV and the C 1s peak of the C(O)O group at 289.9 eV, respectively.[10] The additional peaks at 531.8 and 192.1 eV belong to lattice oxygen (O 1s) and oxidized boron, respectively, in LMB-NBs.[37]

The successful oxidation of aniline monomers to PANI nanofibers (PANI-NFs) was confirmed by FTIR spectroscopy (Figure 1 c). FTIR spectra of PANI-NBs had characteristic peaks at 1140, 1585, and 1499 cm^{-1}, which is a measure of the delocalization of electrons (electronic conductivity) and the stretching vibration of quinoid and benzenoid rings, respectively.[38] The strong bonds at approximately 1312 and 1247 cm^{-1} were attributed to Ph–N and C–NH^+ stretching vibrations, respectively, indicating the presence of emeraldine salts.[26,38]

The surface morphologies of LMB-NBs and PANI-NFs are shown in Figure 2. TEM and SEM images (Figure 2 a) show that the LMB-NBs were composed of several small and highly ordered polycrystalline particles with an even size of 30–40 nm and a uniform size distribution. Moreover, each particle was interconnected through a porous carbon network, forming a web-like morphology. The addition of urea is responsible for constructing the porous carbon network between LMB-NB particles and also effectively suppresses particle growth during synthesis. This porous carbon network not only increases the conductive nature of LMB-NBs, but also allows more electrolyte to be stored within LMB-NBs, thus reducing the distance for the intercalation/deintercalation of lithium ions and augmenting the structural stability against the inherent mechanical stress during high-current cycling. Conversely, worm-like PANI-NFs were obtained during chemical polymerization with a diameter of 50 nm and a length of approximately 500 nm. PANI-NFs also had a uniform size and distribution, exhibiting better capacitive performance.[39] The Brunauer–Emmett–Teller (BET) surface area of LMB-NBs and PANI-NFs was calculated to be about 11 and 63 $m^2 g^{-1}$, respectively. Furthermore, pore-size distribution curves of LMB-NBs and PANI-NFs as a function of pore size, calculated from Barrett–Joyner–Halenda (BJH) analyses (see the Supporting Information, Figure S1 a and b, respectively), confirmed the development of a porous structure of the electrode

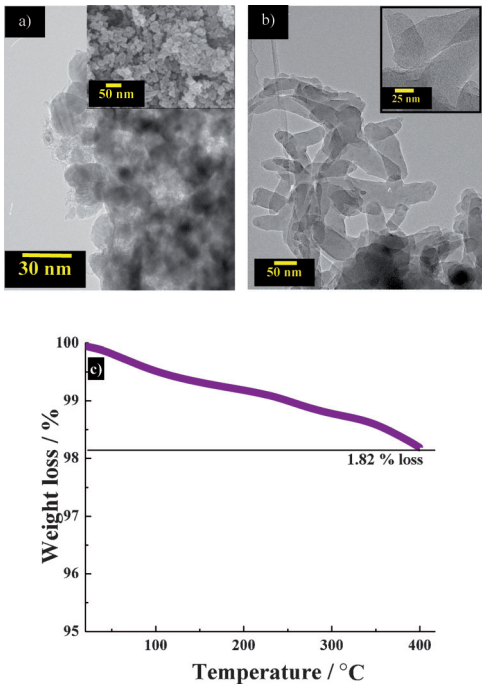

Figure 2. TEM image of a) LMB-NBs and b) PANI-NFs; (c) TGA of LMB-NB powders at 0–400 °C in an air atmosphere. Inset in (a) shows the SEM image of LMB-NBs.

materials, which is a desirable feature for effective ion transportation during the charge–discharge (C/DC) process. Hence, the energy-storage capability of the Li-AHC cell was enhanced. As seen from thermogravimetric analysis (TGA, Figure 2c), the carbon content in LMB-NBs was calculated to be about 1.82%.

Because the applied voltage will split based on the capacitive performance of the individual electrode, when Li-AHC is constructed with different materials with different storage mechanisms, the optimization of the mass balance of each electrode is essential to fabricate high-performance Li-AHCs. Herein, the mass balance of LMB-NB and PANI-NF electrodes for fabricating Li-AHCs were optimized by C/DC studies against the Li counter electrode in $LiPF_6$ (1 M)–EC/DMC electrolyte; corresponding C/DC curves are presented in Figure 3. The C/DC curve of the LMB-NB/Li^+ half-cell (Figure 3a) showed a typical lithium intercalation/deintercalation feature between 1.25 and 4.8 V, whereas the C/DC curve of the PANI-NF/Li^+ cell (Figure 3b) exhibited the charge-storage mechanism based on the doping and undoping of electrolyte active species (PF_6^-) in the range 2–4.5 V. The shape of the C/DC curve is in good agreement with a previous report.[40] A discharge capacitance (DC) of about 93 and 66 mAh g^{-1} was obtained from PANI-NF and LMB-NB electrodes, respectively at 50 mA g^{-1} along with an excellent cyclic life (Figure 3). The better cyclic stability of the LMB-NB anode in the half-cell could be attributed to the presence of a porous carbon network between the LMB-NB particles, which facilitate Li-ion diffusion even at a high-current C/DC process. Moreover, uniformly distributed LMB-NB particles also improved the contact between the particle/particle and the particle/current collector, ensuring the improvement of electrical conductivity; hence lithium-ion-storage capability was enhanced.[23,30] On the other hand, the inherent conductivity and morphological features of PANI-NBs aided its stable electrochemical performance.[33] This prolonged cycling behavior suggested that both PANI-NF and LMB-NB electrodes were compatible for Li-AHC applications in standard inorganic electrolytes. During initial charging, both LMB-NB and PANI-NF electrodes got polarized in the negative and positive direction and started acting as the anode and cathode in a Li-AHC configuration, respectively. Based on the results obtained from Figures 3a and b, the optimized cathode/anode mass ratio for constructing PANI-NF/LMB-NB was about 1.4:1. For comparison, the anodic performance of LMB-NBs was investigated between 0 and 3 V at a 0.25C (60 mA g^{-1}; Figure 3c). The LMB-NB/Li^+ cell delivered a DC of approximately 354 and 220 mAh g^{-1} during the first and second C/DC cycles and maintained 98% of the irreversible capacity value after 50 cycles, which is comparable with the capacity obtained by Ma et al.[31] This excellent anodic performance revealed that LMB-NBs could be utilized as high-performance anode materials for Li-AHCs.

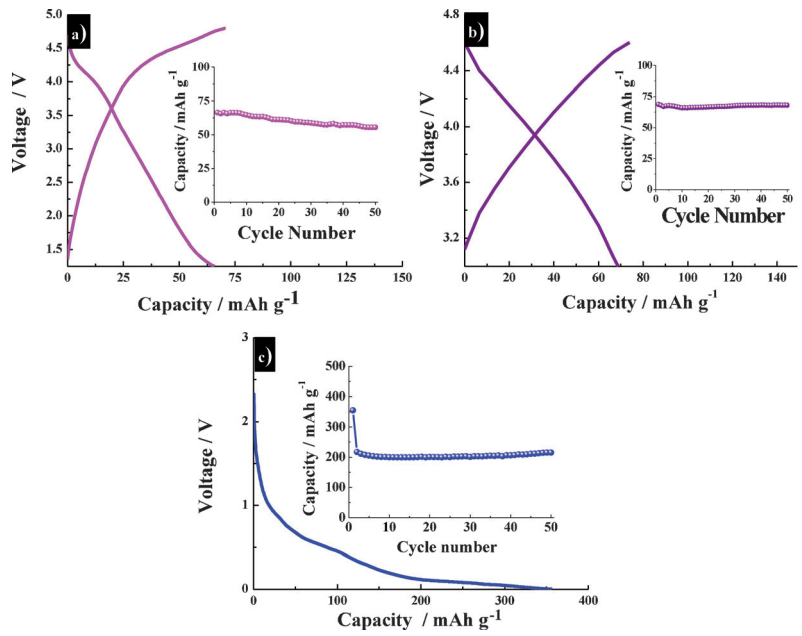

Figure 3. C/DC studies of a) LMB-NB/Li^+ half-cell cycled between 1.25-4.8 V at a current density of 50 mA g^{-1}, b) PANI-NF/Li^+ half-cell cycled between 2–4.5 V at a current density of 50 mA g^{-1}; and c) anodic performance of LMB-NBs at 0–3 V at 0.25C versus the Li counter electrode.

The capacitive performance of the PANI-NF/LMB-NB Li-AHC cell was analyzed by cyclic voltammetry (CV) studies between 0 and 3 V at different scan rates ranging from 1 to 50 mV s^{-1}. The CV curves of Li-AHCs in Figure 4a demonstrate that the PANI-NF/LMB-NB cell displayed an excellent capacitive behavior at all scan rates. Moreover, all CV curves exhibited ideal rectangular curves, with mirror-like images with a rapid current response on voltage reversal at each potential. Additionally, the overlapping of CV curves could be observed at an increasing scan rate, which was attributed to the involvement of the two different energy-storage mechanisms in the PANI-NF/LMB-NB cell.[2] Overall, the storage mechanism of the PANI-NF/LMB-NB cell was mostly based on the doping/undoping of the electrolyte active species (PF_6^-) from the $LiPF_6$ electrolyte (PAN-NF cathode), and the reversible phase transformation that occurred during the Li^+ intercalation reaction (LMB-NB anode).[6,22,23] The shapes of the CV traces showed that capacitance behavior depended on scanning rate.[21,23,27] Specific capacitances of approximately 100, 75, 67, 57, 54, and 50 F g^{-1} were achieved at scan rates of 2, 5, 10, 20, 30, and 50 mV s^{-1}, respectively. Capacitance linearly decreased with an increase in scan rates due to reduced ionic diffusion in the pores at higher scan rates. This occurred because ions could not access the pores and could only approach the outer surface of the electrode materials, thus reducing the uti-

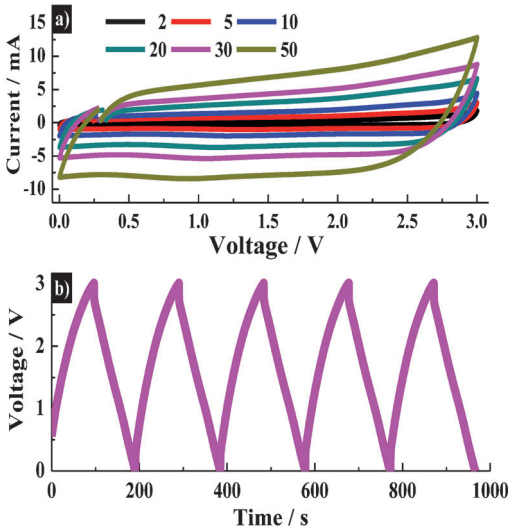

Figure 4. a) CV curves of the PANI-NF/LMB-NB cell in the potential range of 0–3 V at different scan rates; b) C/DC behavior of the PANI-NF/LMB-NB cell at a current density of 1 A g^{-1} between 0 and 3 V in $LiPF_6$ (1 M)–EC/DMC electrolyte.

lization of electroactive species at high scan rates, thereby decreasing the capacitive nature of the Li-AHC cell.[11,21,23,26]

Figure 4b presents the C/DC curves of the PANI-NF/LMB-NB cell at a current density of 1 A g^{-1} in the potential range of 0–3 V. C/DC curves of the Li-AHC cell showed linear and symmetric features as expected. It was thereby validated that the cell had outstanding electrochemical reversibility and capacitive behaviors in $LiPF_6$ (1 M)–EC/DMC electrolyte. Even though an almost linear potential response is shown, C/DC curves are not of an ideal triangular shape; this is attributed to the different energy-storage mechanism involved in charge storage as observed from CV studies.[22,26] It can also be seen from Figure 4b that charge–discharge times of the Li-AHC cell were almost the same, suggesting a 100% columbic efficiency. In addition, an internal resistance (IR) value of 14 Ω was calculated from the C/DC study, indicating low resistance of the PANI-NF/LMB-NB cell. The electrochemical parameters of the Li-AHC cell at different current densities are presented in the Supporting Information (Figure S2) and Table 1. At a current density of 1 A g^{-1}, a DC of approximately 125 F g^{-1} was obtained from the PANI-NF/LMB-NB cell and was maintained at approximately 52 F g^{-1} even at a current density of 3.5 A g^{-1}. Notably, the achieved DC of 125 F g^{-1} at a current density of 1 A g^{-1} is the highest reported for Li-AHCs in organic electrolytes.[14–29,40] This excellent capacitive character of the PANI-NF/LMB-NB cell could be

Table 1. Electrochemical parameters at different current densities.

Current density [A g^{-1}]	DC [F g^{-1}]	ED [Wh kg^{-1}]	PD [W kg^{-1}]
1.00	125	42	1500
1.50	97	32	2150
1.75	71	22	2600
2.25	54	17	3250
3.50	52	16	5350

a result of the presence of the porous carbon network within LMB-NBs and the thinner and more uniform PANI-NFs. More electrolytes were thus able to be trapped within its structure, facilitating the electrode–electrolyte interface and the facile redox reaction, thus improving the capacitive behavior of the Li-AHC cell during prolonged cycling.[21,26,27,39,40] Furthermore, the low IR value and high crystalline nature of LMB-NBs aided the charge storage of the PANI-NF/LMB-NB cell.

To determine electrochemical stability at a high current rate, a C/DC study of the PANI-NF/LMB-NB cell was conducted at 2.25 A g^{-1} for 30000 cycles (Figure 5). All curves were symmetrical and the time difference between the first, 10000th, and 30000th curves was small (Figure 5a), revealing the excellent electrochemical stability of the Li-AHC cell. In addition, a DC of 54 F g^{-1} was obtained at a current density of 2.25 A g^{-1} between 0 and 3 V. Although small fading in capacity was observed for the initial 1000 cycles (Figure 5b), DC was almost constant thereafter, corresponding to 94% of capacitance retention, even after 30000 cycles, along with a coulombic efficiency of >99.5%. To the best of our knowledge, this is the best cyclic performance reported for Li-AHCs fabricated with various lithium intercalating materials at high current rates.[14–27,40–44] This enhanced electrochemical capacitive nature of the PANI-NF/LMB-NB cell might be due to the low IR of the cell and the morphological features of both the cathode and the anode. The porous carbon matrix embedded between the LMB-NB particles, the web-like thinner and uniformly distributed PANI-NFs allowed the accumulation of more electrolytes within the structure of LMB-NBs, providing a flexible structure against inherent mechanical stress during the cycling process at high current rates. An ED of 42 Wh kg^{-1} was obtained at a PD of 1500 W kg^{-1}, and the ED of 16 Wh kg^{-1} was maintained even at a PD of 5350 W kg^{-1} (Table 1). The ED and PD values

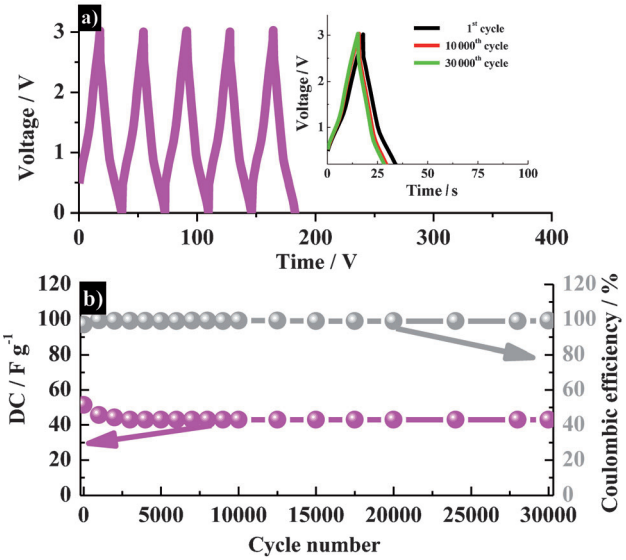

Figure 5. a) C/DC curves and b) cyclic life of the PANI-NF/LMB-NB cell at a current density of 2.25 A g^{-1} for 30000 cycles. Inset in (a) shows the first, 10000th, and 30000th C/DC curves of the Li-AHC cell cycled between 0–3 V.

obtained herein are of particular interest. Table 2 compares ED and PD values of various hybrid systems with those of the PANI-NF/LMB-NB cell, demonstrating the better energy-storage performance of the latter: the PANI-NF/LMB-NB cell outperformed AC/AC, PANI/AC, and prelithiated graphitic electrode/AC systems.[6,16,23,32,34,36] It is well known that constructing electrode materials with improved conductive nature is the best way to increase the energy density of any electrochemical storage device.[10,26,27] It was also reported that the appropriate optimization of electroactive materials is essential for achieving enhanced electrochemical performance at high current rates.[23,26,27]

Table 2. Comparison of energy-storage behavior of the PANI-NF/LMB-NB cell with other Li-AHCs.

System type	ED [Wh kg^{-1}]	PD [W kg^{-1}]	Reference
PANI-NF/LMB-NB	42	1500	this study
AC/PANI	18	1270	[6]
AC/$Li_4Ti_5O_{12}$	10	1000	[14]
AC/$LiMn_2O_4$	38	100	[16,20]
AC/$LiCrTiO_4$	23	800	[17]
AC/V_2O_5	18	235	[18]
AC/TiO_2-B	23	120	[19]
AC/$LiCo_{1/3}Ni_{1/3}Mn_{1/3}O_2$	42	100	[20]
AC/$LiCoO_2$	32	100	[20]
AC/Li_2MnSiO_4	37	1400	[21]
AC/Li_2FeSiO_4	33	1400	[22]
AC/Li_2CoPO_4F	16	1607	[23]
AC/$LiCoPO_4$	11	1607	[23]
carbon nanofoam/$LiCoPO_4$	13	371	[24]
AC/$LiFe_{1/3}Ni_{1/3}Mn_{1/3}O_2$-PANI	30	2000	[26]
AC/$Li_{1.2}(Mn_{0.32}Ni_{0.32}Fe_{0.16})O_2$	23	800	[27]
$Li_4Ti_5O_{12}$/poly(methyl)thiophene	10	30	[34]
AC/AC	3	1600	[16,23,34,36]
MgO-MWCNT/AC	30	220	[41]
($LiMn_2O_4$+AC)/$Li_4Ti_5O_{12}$	16	200	[42]
$LiMn_2O_4$/MnO_2-CNT	42	600	[43]
$LiTi_2(PO_4)_3$/MnO_2	43	200	[44]
CNT/TiO_2-B	12.5	300	[45]

Electrochemical impedance spectroscopy (EIS) studies were performed before and after cycles at a current density of 2.25 A g^{-1} to validate the results obtained from C/DC studies. Nyquist plots of the PANI-NF/LMB-NB cell recorded before and after 30000 C/DC cycles exhibited a semicircle at a high-frequency region and an inclined line at the low-frequency region (Figure 6). In the low-frequency region, the straight line represented the diffusion of lithium ions in the active anode material, which is also related to the Warburg behavior. On the other hand, the depressed semicircle at the high-frequency region is attributed to charge-transfer resistance (R_{ct}).[41] The different R_{ct} values before and after 30000 cycles was small, indicating that the PANI-NF/LMB-NB cell has excellent charge-storage properties, even at high current rates between 0 and 3 V, which agrees well with the results obtained from C/DC studies.

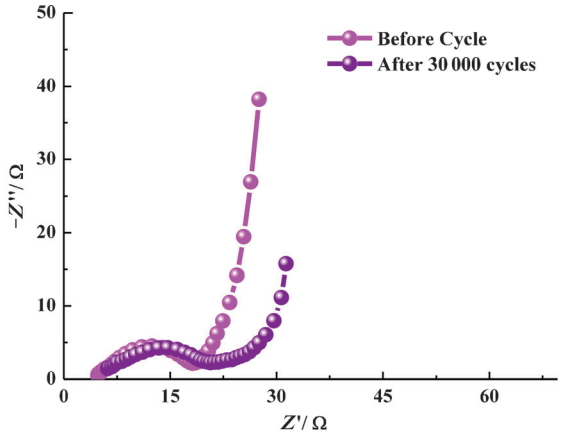

Figure 6. Nyquist plots of the PANI-NF/LMB-NB cell recorded before and after cycles at a current density of 2.25 A g^{-1} for 30000 cycles between 100 kHz and 100 mHz.

Conclusions

We succeeded in adopting monoclinic m (LMB-NBs) as a low-cost/toxicity energy source for fabricating a 3 V high-performance lithium asymmetric hybrid capacitor (Li-AHC) cell along with polyaniline nanofibers (PANI-NFs) as a cathode in a nonaqueous $LiPF_6$ (1 M)–EC/DMC electrolyte. The PANI-NF/LMB-NB cell exhibited outstanding rate performance and excellent electrochemical stability. The Li-AHC cell delivered a discharge capacitance of about 54 F g^{-1} at a current density of 2.25 A g^{-1} and maintained approximately 94% of its initial value after 30000 deep charge–discharge cycles. Furthermore, the PANI-NF/LMB-NB cell delivered an energy density of 42 Wh kg^{-1} at a power density of 1500 W kg^{-1}, which was the best reported energy-storage performance for Li-AHCs fabricated with various lithium insertion hosts. This remarkable rate performance of the hybrid cell is due to its morphological features, the improved electrical conductivity of electrode materials, and the low internal resistance of the cell, suggesting LMB-NBs could be potential candidates for high-rate Li-AHC applications.

Experimental Section

LMB-NBs were prepared using a microwave-assisted irradiation method followed by firing at 650 °C for 7 h in an Ar atmosphere. In typical syntheses, stoichiometric amounts of metal nitrates and boric acid were dissolved in distilled water (100 mL). Then, an appropriate amount of urea was added to the above solution and stirred for 90 min. The molar ratio of metal ions to urea was fixed at 1:10. The resulting solution was heated in a domestic microwave oven for 20 min, and then cooled to room temperature. Finally, the resultant product was fired at 650 °C for 7 h in an Ar atmosphere to give LMB-NB powders. PANI-NFs were synthesized using a chemical polymerization method according to our previous report.[26] Phase analyses of LMB-NBs were performed by XRD measurements (Rint 1000, Rigaku, Japan) equipped with $Cu_{K\alpha}$ as the radiation source. The formation of PANI-NFs was confirmed by FTIR spectroscopy (IRPresitge-21, Japan). BET surface-area analysis was performed using an ASAP 2010 surface analyzer (Micromeritics, USA).

The morphological behavior of LMB-NB and PANI-NF samples was examined by field-emission (FE)-TEM analyses (Tecnai-F20, Philips, the Netherlands) and high-resolution (HR)-SEM (S-4700, Hitachi, Japan). The amount of carbon content in LMB-NBs was determined by TGA from ambient temperature to 400 °C using a thermal analyzer system (STA 1640, Stanton Redcroft Inc., UK). XPS analyses were performed using a Multilab 2000 (UK) instrument with monochromatic AlK_α radiation ($h\nu = 1486.6$ eV).

The electrochemical performance of individual LMB-NBs and PANI-NFs was tested against a lithium counter electrode. Half-cell electrodes were prepared by pressing a slurry of 80 wt% active material (PANI-NFs or LMB-NBs), 10 wt% Ketjenblack (KB) as conductive additive, and a 10 wt% Teflonized acetylene black (TAB) binder on a nickel mesh (200 mm^2) and drying at 160 °C for 4 h in an oven. Half-cells were fabricated in an Ar-filled glove box by sandwiching together a cathode (LMB-NBs or PANI-NFs) and a lithium anode separated by a separator (Celgard 3401) in $LiPF_6$ (1 M) in a mixture of EC and DMC (1:1 *v/v*, Soulbrain Co., Ltd, Korea) electrolytes. The same procedure was also used for PANI-NF/LMB-NB construction, for which LMB-NBs and PANI-NFs were used as the anode and cathode, respectively, after optimizing the mass ratio of electrode materials. Electrochemical measurements (CV and EIS) were conducted using an electrochemical analyzer (SP-150, Bio-Logic, France). C/DC studies of the assembled Li-AHC cell were performed at different current rates between 0 and 3 V using a cycle tester (WBCS 3000, Won-A-Tech, Korea). Electrochemical parameters of the Li-AHC cell, such as DC, IR, ED, and PD were calculated from Equations (2)–(5):[6, 17, 18, 21, 23, 26, 27]

$$DC = 4\,(I\,t/V\,m) \quad (2)$$

$$IR = V_{charge} - V_{discharge}/I \quad (3)$$

$$PD = I\,V/2\,m \quad (4)$$

$$ED = PD\,t/3600 \quad (5)$$

where V_{charge} and $V_{discharge}$ are the potentials at the end of charging and at the beginning of discharge after ohmic drop, respectively, I is the applied current, V is the cell voltage, t is the discharge time, and m is the total mass of electroactive materials, which includes the weight of both cathode and anode.

Keywords: capacitors · electrochemistry · electron microscopy · lithium · polymers

[1] R. Kötz, M. Carlen, *Electrochim. Acta* **2000**, *45*, 2483 – 2498.
[2] M. S. Hong, S. H. Lee, S. W. Kim, *Electrochem. Solid-State Lett.* **2002**, *5*, A227 – A230.
[3] A. Balducci, W. A. Henderson, M. Mastragostino, S. Passerini, P. Simon, F. Soavi, *Electrochim. Acta* **2005**, *50*, 2233 – 2237.
[4] A. Du Pasquier, A. Laforgue, P. Simon, G. G. Amatucci, J. F. Fauvarque, *J. Electrochem. Soc.* **2002**, *149*, A302 – A306.
[5] T. Brousse, R. Marchand, P. L. Taberna, P. Simon, *J. Power Sources* **2006**, *158*, 571 – 577.
[6] J. H. Park, O. O. Park, *J. Power Sources* **2002**, *111*, 185 – 190.
[7] X. Zhao, B. M. Sanchez, P. J. Dobson, P. S. Grant, *Nanoscale* **2011**, *3*, 839 – 855.
[8] C. C. Hu, K. H. Chang, M. C. Lin, Y. T. Wu, *Nano Lett.* **2006**, *6*, 2690 – 2695.
[9] H. L. Wang, J. T. Robinson, G. Diankov, H. J. Dai, *J. Am. Chem. Soc.* **2010**, *132*, 3270 – 3271.
[10] K. Karthikeyan, D. Kalpana, S. Amaresh, Y. S. Lee, *RSC Adv.* **2012**, *2*, 12322 – 12328.
[11] K. Karthikeyan, S. Amaresh, D. Kalpana, R. KalaiSelvan, Y. S. Lee, *J. Phys. Chem. Solids* **2012**, *73*, 363 – 367.
[12] G. Wang, L. Zhang, J. Zhang, *Chem. Soc. Rev.* **2012**, *41*, 797 – 828.
[13] A. D. Pasquier, I. Plitz, J. Gural, F. Badway, G. G. Amatucci, *J. Power Sources* **2004**, *136*, 160 – 170.
[14] I. Plitz, A. D. Pasquier, F. Badway, J. Gural, N. Pereira, A. Gmitter, G. G. Amatucci, *Appl. Phys. A* **2006**, *82*, 615 – 626.
[15] G. G. Amatucci, F. Badway, A. Du Pasquier, T. Zheng, *J. Electrochem. Soc.* **2001**, *148*, A930 – A939.
[16] Y. G. Wang, Y. Xia, *Electrochem. Commun.* **2005**, *7*, 1138 – 1142.
[17] V. Aravindan, W. Chuiling, S. Madhavi, *J. Mater. Chem.* **2012**, *22*, 16026 – 16031.
[18] V. Aravindan, Y. L. Cheah, G. Wee, B. V. R. Chowdari, S. Madhavi, *ChemPlusChem* **2012**, *77*, 570 – 575.
[19] V. Aravindan, N. Shubha, W. Chui Ling, S. Madhavi, *J. Mater. Chem. A* **2013**, *1*, 6145 – 6151.
[20] Y. Wang, J. Luo, C. Wang, Y. Xia, *J. Electrochem. Soc.* **2006**, *153*, A1425 – A1431.
[21] K. Karthikeyan, V. Aravindan, S. B. Lee, I. C. Jang, H. H. Lim, G. J. Park, M. Yoshio, Y. S. Lee, *J. Power Sources* **2010**, *195*, 3761 – 3764.
[22] K. Karthikeyan, V. Aravindan, S. B. Lee, I. C. Jang, H. H. Lim, G. J. Park, M. Yoshio, Y. S. Lee, *J. Alloys Compd.* **2010**, *504*, 224 – 227.
[23] K. Karthikeyan, S. Amaresh, K. J. Kim, S. H. Kim, K. Y. Chung, B. W. Cho, Y. S. Lee, *Nanoscale* **2013**, *5*, 5958 – 5964.
[24] R. Vasanthi, D. Kalpana, N. G. Renganathan, *J. Solid State Electrochem.* **2008**, *12*, 961 – 969.
[25] X. B. Hu, Y. J. Huai, Z. J. Lin, J. S. Suo, *J. Electrochem. Soc.* **2007**, *154*, A1026 – A1030.
[26] K. Karthikeyan, S. Amaresh, V. Aravindan, H. Kim, K. S. Kang, Y. S. Lee, *J. Mater. Chem. A* **2013**, *1*, 707 – 714.
[27] K. Karthikeyan, S. H. Kim, K. J. Kim, S. N. Lee, Y. S. Lee, *Electrochim. Acta* **2013**, *109*, 595 – 601.
[28] J. C. Kim, C. J. Moore, B. Kang, G. Hautier, A. Jain, G. Ceder, *J. Electrochem. Soc.* **2011**, *158*, A309 – A315.
[29] V. Legagneur, Y. An, A. Mosbah, R. Portal, A. L. G. L. Salle, A. Verbaere, D. Guyomard, Y. Piffard, *Solid State Ionics* **2001**, *139*, 37 – 46.
[30] V. Aravindan, K. Karthikeyan, S. Amaresh, Y. S. Lee, *Bull. Korean Chem. Soc.* **2010**, *31*, 1506 – 1508.
[31] R. Ma, L. Shao, K. Wu, M. Lao, M. Shui, C. Chen, D. Wang, N. Long, Y. Ren, J. Shu, *Ceram. Int.* **2013**, *39*, 9309 – 9317.
[32] S. R. Sivakkumar, A. G. Pandolfo, *Electrochim. Acta* **2012**, *65*, 280 – 287.
[33] P. Novák, K. Müller, K. Santhanam, O. Haas, *Chem. Rev.* **1997**, *97*, 207 – 281.
[34] A. Du Pasquier, A. Laforgue, P. Simon, *J. Power Sources* **2004**, *125*, 95 – 102.
[35] D. Salinas-Torres, J. M. Sieben, D. L. Castelló, D. C. Amorósa, E. Morallón, *Electrochim. Acta* **2013**, *89*, 326 – 333.
[36] C. Yu, X. Guan, G. Li, J. Zheng, L. Li, *Scr. Mater.* **2012**, *66*, 300 – 303.
[37] Y. Wang, M. Trenary, *Chem. Mater.* **1993**, *5*, 199 – 205.
[38] Y. Furukawa, F. Ueda, Y. Hyodo, I. Harada, T. Nakajima, T. Kawagoe, *Macromolecules* **1988**, *21*, 1297 – 1305.
[39] J. Huang, *Pure Appl. Chem.* **2006**, *78*, 15 – 27.
[40] E. C. Venancio, A. J. Motheo, F. A. Amaral, N. Bocchi, *J. Power Sources* **2001**, *94*, 36 – 39.
[41] K. Karthikeyan, S. Amaresh, V. Aravindan, Y. S. Lee, *J. Mater. Chem. A* **2013**, *1*, 4105 – 4111.
[42] X. Hua, Z. Denga, J. Suo, Z. Pan, *J. Power Sources* **2009**, *187*, 635 – 639.
[43] S. B. Ma, K. W. Nam, S. B. Yoon, X. Q. Yang, K. Y. Ahn, K. H. Oh, K. B. Kim, *Electrochem. Commun.* **2007**, *9*, 2807 – 2811.
[44] J. Y. Luo, J. L. Liu, P. He, Y. Y. Xia, *Electrochim. Acta* **2008**, *53*, 8128 – 8133.
[45] Q. Wang, Z. Wen, J. Li, *Adv. Funct. Mater.* **2006**, *16*, 2141 – 2146.

Received: February 13, 2014
Revised: March 17, 2014
Published online on ■■ ■■, 0000

K. Karthikeyan, S. Amaresh, S.-N. Lee, J.-Y. An, Y.-S. Lee**

■■ – ■■

High-Power Lithium-Ion Capacitor using $LiMnBO_3$-Nanobead Anode and Polyaniline-Nanofiber Cathode with Excellent Cycle Life

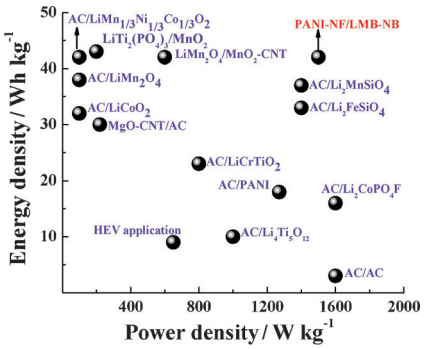

Super performer: A high-performance lithium-ion capacitor (LIC) is fabricated using a $LiMnBO_3$-nanobead anode and a polyaniline-nanofiber cathode in an organic electrolyte. The LIC cell showed superior rate performance investigation relative to other LICs constructed by anodes of various lithium intercalation materials and activated carbon cathodes.